Density-matrix-spectroscopic algorithm for excited-state adiabatic surfaces and molecular dynamics of a protonated Schiff base

E. V. Tsiper, V. Chernyak, S. Tretiak, and S. Mukamel
Department of Chemistry, University of Rochester, Rochester, New York 14627

(Received 7 August 1998; accepted 4 February 1999)

Excited-state potentials of a short protonated Schiff base cation which serves as a model for the photoisomerization of retinal are computed by combining a semi-empirical ground-state adiabatic surface with excitation energies obtained using the time-dependent coupled electronic oscillator (CEO) approach. Excited-state molecular dynamic simulation of the in-plane motion of *cis*-$C_5H_6NH_2^+$ following impulsive optical excitation reveals a dominating $1754\,cm^{-1}$ π-conjugation mode. A new molecular dynamics algorithm is proposed which resembles the Car–Parinello ground-state technique and is based on the adiabatic propagation of the ground-state single-electron density matrix and the collective electronic modes along the trajectory. © *1999 American Institute of Physics.* [S0021-9606(99)30717-0]

I. INTRODUCTION

Photochemical reaction pathways are determined by the evolution of molecules on excited-state adiabatic surfaces $E_\nu(\mathbf{q})$, where $\mathbf{q}$ are the nuclear coordinates. The computation of these surfaces is a formidable task which constitutes the bottleneck in many applications.[1,2]

We have recently proposed an inexpensive method for computing excited-state surfaces.[3] In this approach the ν-th excited-state energy is expressed as

$$E_\nu(\mathbf{q}) = E_0(\mathbf{q}) + \Omega_\nu(\mathbf{q}). \tag{1}$$

The ground-state energy $E_0(\mathbf{q})$ is computed using any standard quantum-chemistry technique, while the excitation energy $\Omega_\nu(\mathbf{q})$ is obtained using the Coupled Electronic Oscillator (CEO) approach[4,5] that targets directly the linear response of the system, avoiding the costly computation of excited-state many-electron wave functions. Normally one first computes potential surfaces and then uses them to compute spectra. Here we reverse these steps: we first compute adiabatic spectra and then use them to generate the adiabatic surfaces of the optically active states at the relevant nuclear configurations. Excited-state surfaces of short polyenes which compare well with *ab initio* calculations and reproduce the experimental resonant Raman spectra were obtained using this technique.[3]

In this paper we employ this algorithm to perform molecular dynamics simulations for the photoexcited *cis*-$C_5H_6NH_2^+$ protonated Schiff base cation (see Fig. 1). This molecule has been used as a ''minimal model'' for retinal photoisomerization.[6] The photochemistry of retinal and its derivatives is one of the most important problems in photobiology, since this chromophore is responsible for photoreception in vision.[7] A protein of the opsin family changes its conformation upon the absorption of a single photon by an embedded Schiff base of retinal. There has been a considerable interest in the origin of the extremely fast rate and the high quantum yield of the photoisomerization of retinal, which is one of the fastest known in nature.[8–10] This photochemical reaction was studied using a broad range of spectroscopic techniques[11] both in solution and in a natural state inside a protein core. Continuous-wave and long-time nanosecond to picosecond studies include linear absorption,[12,13] resonant Raman,[14] infrared,[15] hole burning,[12] second-order polarizabilities,[16] and two photon absorption.[17] More recently a broad variety of sub-picosecond and femtosecond spectroscopies were applied. These include pump–probe,[18–30] optical pump—infrared probe,[31] time and frequency resolved fluorescence,[32–35] and time-resolved Raman.[36,37]

Early time-resolved experiments[38] estimated the rhodopsin (11-*cis*) to bathorhodopsin (all-trans) photoconversion time scale to be about 3 ps. Shorter optical pulses have revealed two transients that precede the bathorhodopsin formation and appear on the time scale of 200 fs.[27] Subsequent experiments[25,26] have in contrast suggested that the isomerization photoproduct is fully formed within 200 fs. Strong coupling to the torsional degree of freedom has been proposed to cause fast and vibrationally coherent departure from the Frank–Condon region.[23] This conclusion has been questioned by the recent experiments[39] involving retinal where the photoisomerization pathway has been blocked. Comparison of the photoisomerization dynamics of different retinal isomeres[24] and substituents[40] indicates that the high photoisomerization rate and quantum yield are closely connected. These results are commonly interpreted using a two-level picture (ground-state+one optically-allowed excited state)[41,42] whereby the photoisomerization process is described as Landau–Zener tunneling.[32,24] Transient stimulated emission experiments support this model.[43]

Despite these extensive studies, a complete understanding of this process is yet to be developed. There seem to be several viewpoints onto both the origin of the fast photoreaction and the description of relevant electronic and vibrational states. Recent pump–dump–probe experiments[21,20] have been interpreted by assuming that a third, optically dark, state participates in the photoisomerization process.

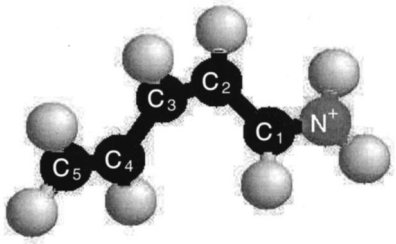

FIG. 1. Protonated Schiff base *cis*-$C_5H_6NH_2^+$.

This state is believed to be responsible for the two-photon absorption reported in Ref. 17. The second excited-state has been taken into account in recent theoretical simulations.[44] The role of the conical intersection point in the photoisomerization process has drawn considerable attention[45,46] Existence of a barrierless path to adiabatic surface crossing has been shown for short protonated Schiff bases[47] as well as for related conjugated hydrocarbons.[48]

Recent femtosecond resonant Raman measurements show that an in-plane motion along the conjugated length is the primary event which precedes the photoisomerization.[36] An in-plane primary step of the photoreaction has also been proposed in Ref. 6, where a minimal energy path for the photoisomerization of *cis*-$C_5H_6NH_2^+$ has been computed using *ab initio* CI calculations. These calculations show that the minimal energy path to the crossing point starts with an in-plane bond stretching, while photoisomerization only takes place after the bond stretching is completed. The picture of bond stretching prior to isomerization is consistent with the observation of linear dependence between the linear absorption maximum and Raman shift of the conjugation vibrational mode.[49]

Car–Parinello molecular dynamics of a stand-alone retinal molecule using *ab initio* ground-state adiabatic surface with an external torsional potential was performed in Ref. 50. Extensive molecular-dynamics simulation of the entire Bacteriorhodopsin protein with the retinal embedded in it were performed using CHARMm force field.[51,41,52,42] Recently the force field was improved by adjusting the torsional potential to match CASSCF *ab initio* calculation for a short retinal analogue, and by using a density-matrix description of avoided level crossing.[44]

In Sec. II we outline briefly the CEO algorithm and present a slice of the lowest five potential surfaces of the short protonated Schiff base computed along the dihedral angle, keeping all other coordinates fixed. Excited-state molecular dynamics simulation of the in-plane motion performed in Sec. III demonstrates the dominant role of the conjugation mode on the 200 fs time scale. In Sec. IV we discuss these results and further propose a computationally efficient analytical procedure to calculate the excited-state adiabatic surface derivatives with respect to the nuclear coordinates. This results in a molecular dynamics algorithm which computes the excited state only once at a starting nuclear configuration. The excited-state surface is then generated ''on the fly'' by propagating the CEO modes (Appendices A–D).

The present propagation of modes bears close analogy with the Car–Parinello molecular dynamics technique for the ground state,[53] whereby the electronic structure is propagated in time together with the nuclear configuration using fictitious classical equations of motion. The present method follows the true evolution of the system within the TDHF approximation and no fictitious equations of motion are introduced. However, the analogy with Car–Parinello lies in the propagation of the electronic structure in time which avoids repetitive solution of the TDHF at every new nuclear configuration. Given the low computational cost of CEO calculations, we anticipate the possibility of performing large-scale excited-state molecular-dynamic calculations, taking into account the surrounding solvent and protein.

II. ADIABATIC POTENTIALS ALONG THE ISOMERIZATION COORDINATE

The CEO is a reduced description of electronic structure which only uses a small amount of relevant excited-state information and is based on the time-dependent single-electron density matrix of the molecule interacting with an external optical field $\mathcal{E}(t)$:[54]

$$\rho_{ij}(t)=\langle\Psi(t)|c_i^\dagger c_j|\Psi(t)\rangle. \tag{2}$$

Here $\Psi(t)$ is the many-electron wave function and $c_i^\dagger$ (c_i) are the fermionic creation (annihilation) operators for the atomic orbital i. The diagonal elements $\overline{\rho_{ii}}(t)$ give the electronic charge distribution across the molecule. Density-functional theory (DFT)[55–62] only retains the diagonal elements $\overline{\rho_{ii}}=\langle 0|c_i^\dagger c_i|0\rangle$, where $|0\rangle$ denotes the many-electron ground-state. The off-diagonal elements of the density matrix carry additional information about *electronic coherences*[5] which is vital for computing optical excitations. When the molecule is driven by an external field, its wave function $|\Psi(t)\rangle$ and the single-electron density matrix $\rho(t)\equiv\overline{\rho}+\delta\rho(t)$ become time-dependent. The field-induced component of the density matrix $\delta\rho(t)$ can be computed by solving the Heisenberg equations of motion for $c_i^\dagger c_j$. The hierarchy of many-body dynamics is closed by invoking the time-dependent Hartree–Fock (TDHF) ansatz ($|\Psi(t)\rangle$ is represented by a single Slater determinant at all times), resulting in closed nonlinear equations of motion for $\delta\rho(t)$.[63] $\delta\rho(t)$ is further expanded in the eigenmodes ξ_ν of the Liouville operator $\hat{L}$ (Appendices A and B)

$$\hat{L}(\mathbf{q})\xi_\nu(\mathbf{q})=\Omega_\nu(\mathbf{q})\xi_\nu(\mathbf{q}), \tag{3}$$

which gives

$$\delta\rho(t)=\sum_\nu a_\nu(t)\xi_\nu+\sum_\nu a_\nu^*(t)\xi_\nu^\dagger. \tag{4}$$

The eigenvalues $\Omega_\nu(\mathbf{q})$ provide the excitation frequencies. The electronic normal mode $\xi_\nu(\mathbf{q})$ is an approximation to the transition density matrix between the ground $|0\rangle$ and excited $|\nu\rangle$ states:[64] $(\xi_\nu)_{ij}=\langle 0|c_i^\dagger c_j|\nu\rangle$.

Solution of Eq. (3) at various nuclear configurations $\mathbf{q}$ yields the $\mathbf{q}$-dependent excitation energies Ω_ν. The excited-state adiabatic surface $E_\nu(\mathbf{q})$ is obtained using Eq. (1) by adding $\Omega_\nu(\mathbf{q})$ to the ground-state adiabatic surface

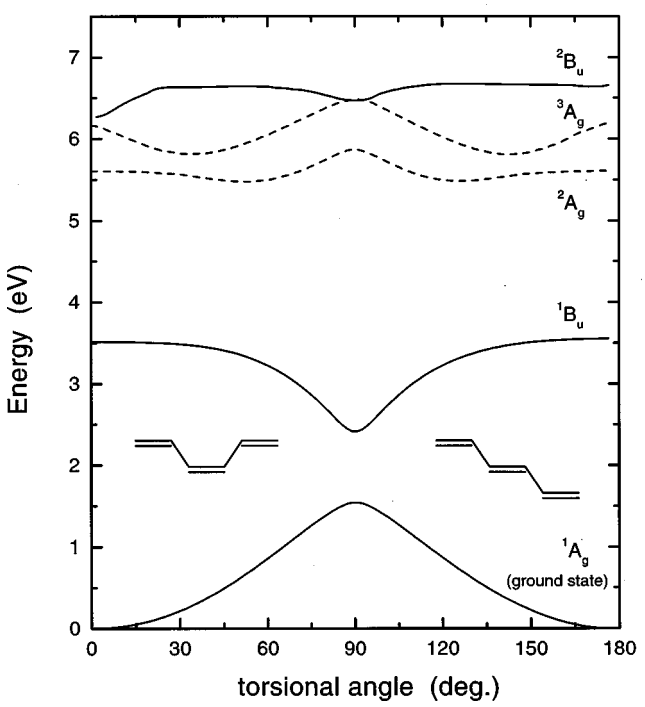

FIG. 2. Ground- and four lowest excited-state adiabatic surface slices along the C_1–C_2–C_3–C_4 torsional angle coordinate. All other internal coordinates are held fixed at the *cis* equilibrium values. The apparent *cis* and *trans* degeneracy is accidental; the *trans*-geometry is not the optimal geometry and therefore have the ground-state energy higher than the energy in the true minimum.

$E_0(\mathbf{q})$, which is an input to this calculation. Finally, the adiabatic linear polarizability is given in terms of $\Omega_\nu(\mathbf{q})$ and the transition dipole moment $\boldsymbol{\mu}^{0\nu}(\mathbf{q})=\mathrm{tr}\{\boldsymbol{\mu}(\mathbf{q})\xi_\nu(\mathbf{q})\}$ as

$$\alpha(\omega;\mathbf{q})=\sum_\nu \frac{\gamma|\boldsymbol{\mu}^{0\nu}(\mathbf{q})|^2}{(\omega-\Omega_\nu(\mathbf{q}))^2+\gamma^2}, \tag{5}$$

where γ is a homogeneous dephasing rate.

The AM1 semiempirical ground-state energy surface $E_0(\mathbf{q})$ was obtained using Gaussian 94.[65] The ground-state electronic density matrix $\overline{\rho}(\mathbf{q})$ and INDO/S Hamiltonian parameters were then computed using ZINDO.[66] Finally, the DSMA procedure[67] was applied to calculate the excitation energies Ω_ν.

We started with the AM1 *cis*-optimized geometry and then varied the C_1—C_2—C_3—C_4 torsional angle ϕ, keeping all other internal coordinates fixed. $\phi=0$ and 180° correspond to *cis* and *trans* conformations, respectively. We have used this algorithm to find four excited states of the *cis*-$C_5H_6NH_2^+$ cation along the *cis*- to *trans*-isomerization coordinate. The resulting potential slices are displayed in Fig. 2 (only the interval $0\leqslant\phi\leqslant180°$ is shown since the potential is symmetric around $\phi=0$). The optically-allowed B_u type states are depicted by solid curves, whereas the almost forbidden A_g type states are given by dashed curves.[68]

The lowest excitation energy of 3.5 eV at $\phi=0$ compares well with 90 kcal/mol ($\approx$3.9 eV) of Ref. 6. The potentials shown in Fig. 2 are in a good agreement with the results for larger protonated Schiff base obtained using complete active space self-consistent field (CASSCF).[44] The noticeably larger second excitation energy may be attributed to the shorter size of the present molecule.[69,70] The ratio of the excitation energies $\Omega_2/\Omega_1=1.59$ at $\phi=0$ agrees with the CIS *ab initio* result of 1.51, obtained at 6-31+G level using Gaussian 94.[71] The adiabatic excitation energy reduces threefold at $\phi=90°$, indicating that this configuration is very close to the conical crossing point, predicted by Olivucci *et al.*[6] Since the excited-states are nondegenerate, the gradient of the excited-state potentials with respect to the torsional angle is zero at $\phi=0$.

III. IN-PLANE MOLECULAR DYNAMICS SIMULATION: THE EFFECTIVE CONJUGATION COORDINATE

We have simulated the vibrational dynamics of the photoexcited protonated Schiff base on the lowest excited state $E_1(\mathbf{q})$ surface. The simulation started with the AM1 ground-state equilibrium geometry $\mathbf{q}_0$. Assuming an impulsive optical excitation, the molecule finds itself on the $E_1(\mathbf{q})$ surface at $\mathbf{q}=\mathbf{q}_0$ (vertical Frank–Condon transition). Vibrational motions and relaxation start because this geometry does not correspond to the minimum of the excited-state surface. We have used the ground-state normal modes as a coordinate system. The position of the n-th nucleus is then expanded as

$$\mathbf{r}_n(t)=\mathbf{r}_n^{(0)}+\sum_{\alpha=1}^{3K-6}\mathbf{d}_{n\alpha}Q_\alpha(t). \tag{6}$$

Here K is the number of nuclei, $\mathbf{r}_n^{(0)}$ is its ground-state equilibrium position, and $\mathbf{d}_{n\alpha}$ is the transformation matrix for the ground state normal modes. Both $\mathbf{r}_n^{(0)}$ and $\mathbf{d}_{n\alpha}$ are obtained from ground-state AM1 calculation. The normal mode amplitudes $Q_\alpha(t)$ are calculated by solving the classical equations of motion

$$M_\alpha\ddot{Q}_\alpha=-\frac{\partial E_1}{\partial Q_\alpha}, \tag{7}$$

where M_α is the mass of the α-th normal mode, with the initial condition $Q_\alpha(0)=0$, $\dot{Q}_\alpha(0)=0$. The derivatives in the right-hand side of Eq. (7) were obtained by numerical differentiation using $\Delta q=0.01$ Å. Equation (7) was integrated using Runge–Kutta–Fehlberg method of 4–5-th order[72] with the effective time step of 0.33 fs, and the trajectory was computed for 400 fs. The calculation was repeated with half the time step and the relative error in bond lengths at the end of the time interval was found to be about 10^{-4}. The present molecular dynamics simulation takes approximately 11 real-time seconds per 1 fs of evolution time.[73]

The molecule starts evolving according to Eq. (7). By symmetry, the energy gradient is nonzero only for the fully symmetric modes, and planar symmetry is therefore maintained throughout the simulation. Classical in-plane motion is preserved even when the molecule is unstable with respect to out-of-plane modes. Thus, in order to induce isomerization one needs to drive the molecule out of the planar geometry by adding an out-of-plane driving force.[50] Since the planar geometry is preserved, the actual number of degrees of freedom was reduced from $3K-6=36$ to $2K-3=25$.

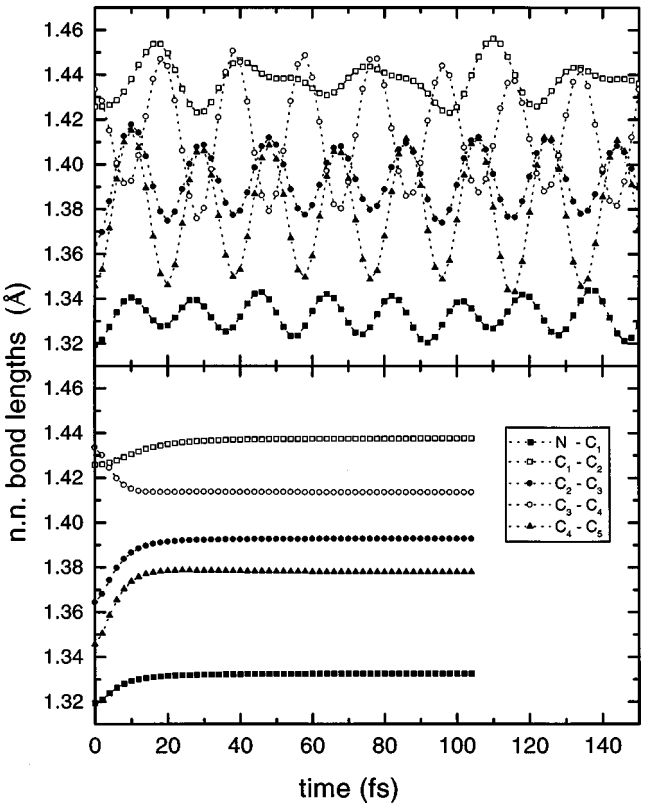

FIG. 3. Upper panel: time evolution of the bond lengths between heavy atoms following an impulsive optical excitation. Lower panel: same calculation but with a critical damping introduced into the classical equations of motion.

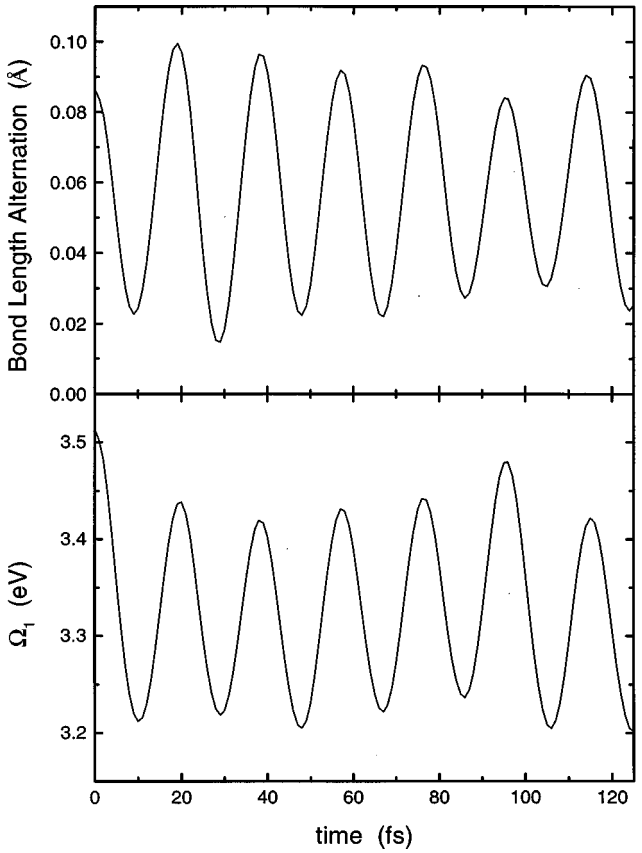

FIG. 4. Evolution of (a) bond length alternation parameter and (b) adiabatic excitation energy Ω_1 following an impulsive optical excitation.

The upper panel of Fig. 3 shows the time dependence of all heavy-atom bond lengths. A dominant mode with 19 fs period ($1754\,\mathrm{cm}^{-1}$) is observed. This mode corresponds to shortening the single bonds and elongating the double bonds, such that 9.5 fs after the excitation the single and double C–C bonds are interchanged, in agreement with recent experimental observations.[36] These changes in molecular geometry can be represented by the bond length alternation parameter (BLA) shown in Fig. 4(a)

$$S=(l_{\mathrm{NC}_1}+l_{\mathrm{C}_2\mathrm{C}_3}+l_{\mathrm{C}_4\mathrm{C}_5})/3-(l_{\mathrm{C}_1\mathrm{C}_2}+l_{\mathrm{C}_3\mathrm{C}_4})/2, \tag{8}$$

where l_{mn} denotes the bond length between atoms m and n. This is the average difference between single and double bonds. The fundamental period seen in the BLA is 19 fs. For comparison, the main period of the N–H bond in Fig. 4 is 9.8 fs ($3415\,\mathrm{cm}^{-1}$). A strong correlation between BLA and the adiabatic excitation energy $\Omega_1(t)$ [Fig. 4(b)] is observed. This is a consequence of the fact that the excitation energy of a π-conjugated system depends crucially on the conjugation length. This observation forms the basis for the Effective Conjugation Coordinate (ECC) model for vibrational spectra of polyconjugated molecules.[49] This model introduces a collective vibrational coordinate strongly coupled to π-electrons (R mode) which in the case of polyenes coincides with the BLA parameter. R describes a collective oscillation that moves nuclei from the ground electronic state geometry to the optimal geometry of the first excited electronic state. The ECC model provides a clear interpretation of infrared and Raman spectra of many conjugated molecules.[49]

The upper panel in Fig. 5 presents the time-evolution of the normal mode amplitudes $Q_\alpha(t)$. This molecular-dynamics algorithm can also be used to obtain the excited-state equilibrium geometry. The lower panel in Fig. 5 demonstrates the convergence of the normal mode amplitudes to the excited-state equilibrium values when a classical friction term $-\gamma_\alpha \dot{Q}_\alpha$ is added to the right-hand side of Eq. (7). The critical damping $\gamma_\alpha = 2\omega_\alpha / M_\alpha$ was chosen to minimize the cooling time which is then approximately equal to one oscillation period of the corresponding mode. The simulation time (about 400 fs) necessary to obtain the excited-state equilibrium geometry is thus determined by the lowest-frequency mode (Fig. 5).

We note, however, that low-frequency vibrational modes hardly affect the local arrangement of nuclei, which is usually associated with high-frequency modes. Thus the nearest-neighbor bond lengths and angles converge faster than the true energy minimum. The lower panel on Fig. 3 shows the convergence of the C–C bond lengths which occurs at about 20 fs, i.e., one period of the dominant vibration.

Figure 6 displays the energies associated with the vibrational normal modes

$$W_\alpha(t)=\frac{M_\alpha}{2}[\dot{Q}_\alpha^2(t)+\omega_\alpha^2 Q_\alpha^2(t)]. \tag{9}$$

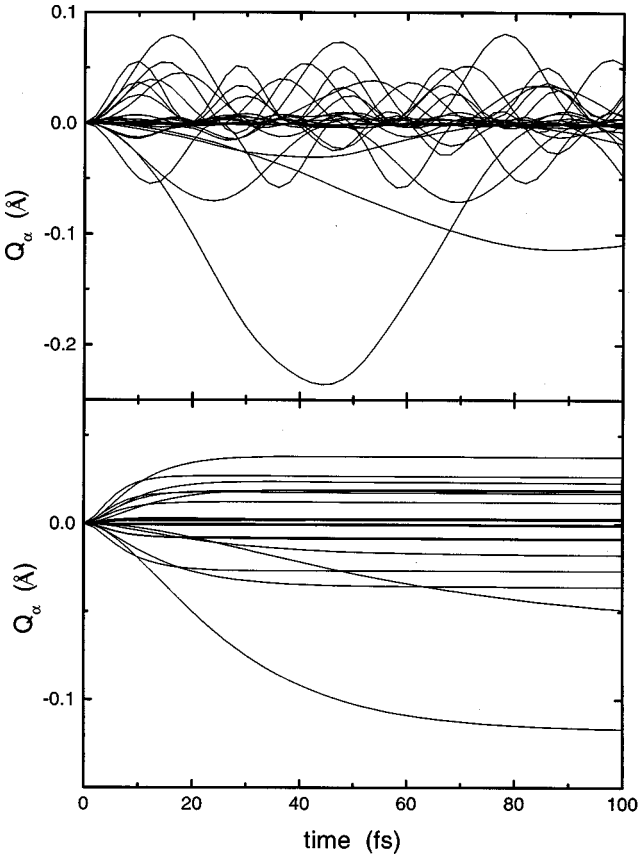

FIG. 5. Upper panel: evolution of the normal mode amplitudes $Q_\alpha(t)$ [Eq. (6)]. Lower panel: the same quantities when critical damping is introduced into the classical equations of motion.

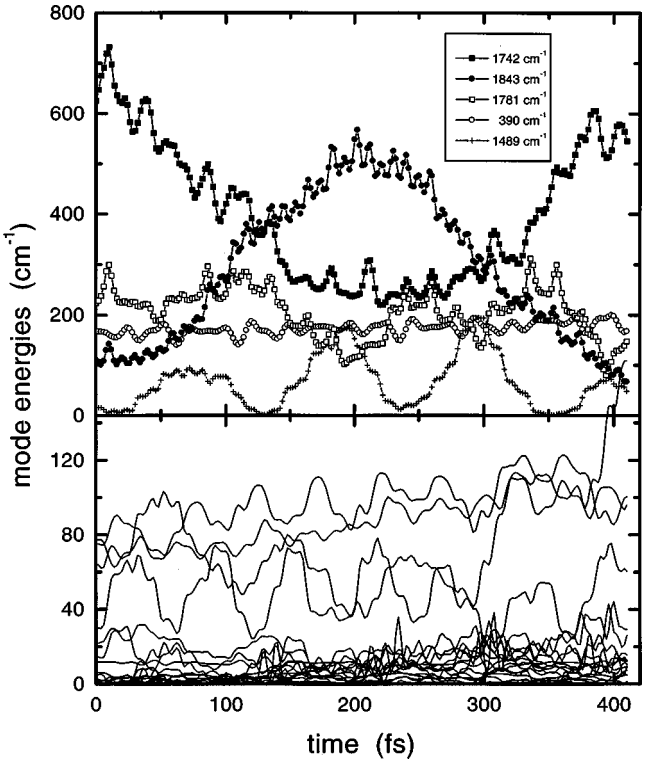

FIG. 6. Total (kinetic+potential) energies $W_\alpha(t)$ [Eq. (9)] of the normal modes. The five most highly excited modes are displayed on the upper panel, while the lower panel shows the remaining modes. Slow intramolecular vibrational redistribution is due to a weak anharmonicity of the excited-state adiabatic surface.

Here ω_α is the frequency of the nuclear mode α. The upper panel displays the five most highly excited modes while the lower panel shows the remaining 21 normal modes with energies less than $120\,\mathrm{cm}^{-1}$. The power spectrum is clearly dominated by two modes with frequencies 1742 and $1843\,\mathrm{cm}^{-1}$ which are close to the dominant frequency seen in the BLA. Thus, a combination of these modes could be identified as the Effective Conjugation Coordinate (ECC).[49] Both modes are associated with the bond length alternation as can be clearly seen from the atomic displacements depicted in Fig. 7. Intramolecular vibrational redistribution is induced by the E_1 surface anharmonicity. The present dynamical picture is not limited to the specific Schiff base studied here. We have also observed the dominant role of the ECC mode in all-trans configuration of the same Schiff base, in cis- and trans-hexatriene and in cyclohexadiene.

IV. DISCUSSION AND EXTENSIONS

The present excited-state molecular-dynamics technique uses potential surfaces obtained from inexpensive calculations of adiabatic spectra. This method should be particularly useful in the study of photochemical reaction pathways of large molecules.

The TDHF approximation using semi-empirical INDO/S Hamiltonian gives reasonable accuracy in the description of optical excitations of a large variety of molecules.[67,74,5,75,76] Good accuracy of the excited-state adiabatic surfaces, vibronic modes and excited-state geometry of short polyenes has been obtained in Ref. 3, compared with *ab initio* CIS calculations using sufficiently large basis sets. Although a better accuracy for the excited states may be reached using more elaborate treatments, this usually requires a considerably greater computational effort, incompatible with the requirements set by molecular-dynamics simulations. A notable advantage of the present approach is also in that we do not need to compute one excited state at a time, since many states are generated simultaneously.

The classical description of nuclear motions is exact for harmonic vibrational modes and should hold for anharmonic

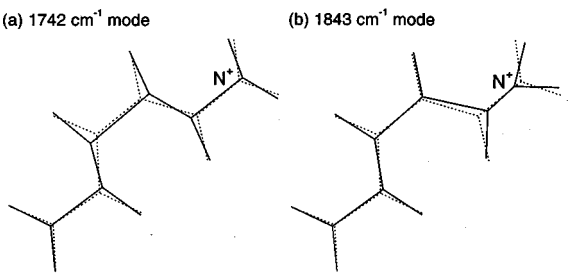

FIG. 7. Schematic depiction of atomic displacements associated with two dominant modes seen in Fig. 5. Solid lines give the equilibrium atomic positions, and dotted line show the positions of atoms, when the corresponding mode amplitude is 0.5 Å.

modes as long as their energies are higher than their vibrational quantum $\hbar\omega_\alpha$. Good accuracy is thus expected for low-frequency modes. Our results for high-frequency modes therefore hold provided their anharmonicities are small. However, the isomerization process, (which was not simulated here) involves a high energy in the low-frequency torsional coordinate (see Fig. 2), where the classical picture should apply even for strong anharmonicities.

A fully quantum treatment of high-frequency vibrations requires diagonalization of the excited-state Hamiltonian and can only be done for small systems. For larger systems, wave-packet propagation techniques can be used.[77] The present technique can serve as an ingredient of these methods for computing the excited-state potentials in relevant nuclear configurations.

The bottleneck in the present molecular-dynamics simulations is the repetitive computation of $E_\nu(\mathbf{q})$ at each nuclear configuration $\mathbf{q}$, since the right-hand side of Eq. (7) needs to be evaluated at every time step. Usually an empirical ground-state potential energy function is used in ground-state molecular dynamics calculations,[78] as implemented, e.g., in the CHARMm code.[79] A combination of CHARMm potential with a one-dimensional slice of a first-principle excited-state potential along the torsional coordinate was used recently in the molecular-dynamics simulation of bacteriorhodopsin.[44] Analytic derivative techniques are commonly employed in quantum chemistry calculations[65,80] to reduce computational cost. In these techniques the HF or CI calculation is carried out only once for the equilibrium configuration $\mathbf{q}_0$, and the solution is expanded analytically in its vicinity.[81–83] This results in the Coupled-Perturbed Hartree–Fock (CPHF) equations. An analogous procedure, the coupled-perturbed collective electronic oscillator (CPCEO), which computes the excited-state adiabatic surface using *ab initio* or semi-empirical electronic Hamiltonian by propagation of the Hamiltonian, is developed in Appendices C and D. In Appendix B we outline the spectral properties of the superoperator $\hat{L}$ necessary to derive the perturbation theory for its eigenmodes ξ_ν and eigenfrequencies Ω_ν. These properties are then used in Appendix C for the analytic derivatives procedure for computing first and second derivatives of the CEO excitation energy at a given nuclear configuration $\mathbf{q}$. These make it possible to obtain the derivatives of the CEO solution with respect to nuclear coordinates by solving the CEO equations only once at this $\mathbf{q}$.

Let $\mathbf{q}$ denote the set of mass-weighted nuclear coordinates. Then, a classical trajectory is computed by propagating the following system of CPCEO equations:

$$\frac{\partial^2\mathbf{q}}{\partial t^2}=-E_0^{\mathbf{q}}-\Omega_\nu^{\mathbf{q}}, \tag{10a}$$

$$\frac{\partial\overline{\rho}}{\partial t}=\overline{\rho}^{\mathbf{q}}\frac{\partial\mathbf{q}}{\partial t}, \tag{10b}$$

$$\frac{\partial\xi_\nu}{\partial t}=\xi_\nu^{\mathbf{q}}\frac{\partial\mathbf{q}}{\partial t}. \tag{10c}$$

Here a $\mathbf{q}$ superscript denotes a derivative with respect to $\mathbf{q}$. The ground-state potential gradients $E_0^q=E_0^{\mathbf{q}}(\overline{\rho};t^{\mathbf{q}},V^{\mathbf{q}})$ are calculated (see Appendix C) as

$$E_0^{\mathbf{q}}=2\,\mathrm{tr}(\overline{\rho}t^{\mathbf{q}}+\tfrac{1}{2}\overline{\rho}\hat{V}^{\mathbf{q}}\overline{\rho}). \tag{11}$$

The excitation energy gradients $\Omega_\nu^{\mathbf{q}}=\Omega_\nu^{\mathbf{q}}(\overline{\rho},\xi_\nu;\overline{\rho}^{\mathbf{q}},t^{\mathbf{q}},V^{\mathbf{q}})$ are obtained using Eq. (D3):

$$\Omega_\nu^{\mathbf{q}}=(\xi_\nu|[t^{\mathbf{q}}+\hat{V}^{\mathbf{q}}\overline{\rho},\xi_\nu]+[\hat{V}^{\mathbf{q}}\xi_\nu,\overline{\rho}]+[\hat{V}\overline{\rho}^{\mathbf{q}},\xi_\nu]+[\hat{V}\xi_\nu,\overline{\rho}^{\mathbf{q}}]|\xi_\nu). \tag{12}$$

The ground-state density matrix gradients $\overline{\rho}^{\mathbf{q}}=\rho^{\mathbf{q}}(\overline{\rho};t^{\mathbf{q}},V^{\mathbf{q}})$ are calculated by solving CPHF linear system (see Appendix C)

$$\hat{L}\overline{\rho}^{\mathbf{q}}=[\overline{\rho},t^{\mathbf{q}}+\hat{V}^{\mathbf{q}}\overline{\rho}]. \tag{13}$$

Finally the gradients of the collective electronic modes $\xi_\nu^{\mathbf{q}}=\xi_\nu^{\mathbf{q}}(\overline{\rho},\xi_\nu;\overline{\rho}^{\mathbf{q}},t^{\mathbf{q}},V^{\mathbf{q}})$ are computed using Eq. (D6) by solving the equation

$$(\hat{L}-\Omega_\nu)\xi_\nu^{\mathbf{q}}=([t^{\mathbf{q}}+\hat{V}^{\mathbf{q}}\overline{\rho},\xi_\nu]+[\hat{V}^{\mathbf{q}}\xi_\nu,\overline{\rho}]-\Omega_\nu^{\mathbf{q}}+[\hat{V}\overline{\rho}^{\mathbf{q}},\xi_\nu]+[\hat{V}\xi_\nu,\overline{\rho}^{\mathbf{q}}])\xi_\nu. \tag{14}$$

The arguments in these expressions show the explicit dependence on the relevant variables $(\overline{\rho},\xi_\nu;\overline{\rho}^{\mathbf{q}},t^{\mathbf{q}},V^{\mathbf{q}})$. For example, computing $E_0^{\mathbf{q}}$ using the CPHF [Eq. (11)] requires $\overline{\rho}$ and the derivatives $t^{\mathbf{q}}$ and $V^{\mathbf{q}}$ of the matrix elements, while obtaining $\Omega_\nu^{\mathbf{q}}$ using CPCEO [Eq. (14)] requires also ξ_ν and $\overline{\rho}^{\mathbf{q}}$. The proposed CPCEO analytic derivatives procedure yields the excited-state surface in the vicinity of a given nuclear configuration. Using these equations, the CEO calculation should be carried out only once at the beginning of the simulation and the electronic ground state $\overline{\rho}$ and modes ξ_ν are propagated along the trajectory, in the spirit of the Car–Parinello approach for ground-state simulations.[53] The absence of long range electronic coherence may be used to reduce the number of density matrix elements from $\sim N^2$ to $\sim N\times N_c$ where the coherent size N_c denotes the number of orbitals of closely lying atoms.[84,85] A favorable linear N-scaling of computational effort with size is then possible, since typically $N_c\ll N$. This is analogous to similar developments in ground state calculations.[86,87]

ACKNOWLEDGMENTS

We gratefully acknowledge the support of the National Science Foundation and the Air Force Office of Scientific Research.

APPENDIX A: THE CEO ALGORITHM

We consider the adiabatic molecular Hamiltonian for a molecule driven by an external field $\mathcal{E}(t)$[62]

$$H=\sum t_{ij}c_{i\sigma}^\dagger c_{j\sigma}+\sum\langle ij|kl\rangle c_{j\sigma}^\dagger c_{i\sigma'}^\dagger c_{k\sigma'}c_{l\sigma}-\boldsymbol{\mathcal{E}}(t)\sum\boldsymbol{\mu}_{ij}c_{i\sigma}^\dagger c_{j\sigma}. \tag{A1}$$

The first two terms represent the free molecule, whereas the last term describes the coupling to an external optical electric field $\boldsymbol{\mathcal{E}}(t)$. Single-electron matrix elements t_{ij}, Coulomb matrix elements $\langle ij|kl\rangle$, and dipole moment matrix elements $\boldsymbol{\mu}_{ij}$ may be expressed in terms of the atomic orbitals $\chi_{i\sigma}(\mathbf{r})$ as

$$t_{ij}=\int d\mathbf{r}\,\chi_i^*(\mathbf{r})[\Delta_{\mathbf{r}}+v_{\text{core}}(\mathbf{r})]\chi_j(\mathbf{r}), \tag{A2a}$$

$$\langle ij|kl\rangle=\int\int d\mathbf{r}\,d\mathbf{r}'\,\chi_i^*(\mathbf{r})\chi_j^*(\mathbf{r}')|\mathbf{r}-\mathbf{r}'|^{-1}\chi_k(\mathbf{r})\chi_l(\mathbf{r}'), \tag{A2b}$$

$$\boldsymbol{\mu}_{ij}=\int d\mathbf{r}\,\chi_i^*(\mathbf{r})\mathbf{r}\chi_j(\mathbf{r}). \tag{A2c}$$

Here v_{core} is the potential created by atomic cores. All matrix elements t_{ij}, $\langle ij|kl\rangle$, and $\boldsymbol{\mu}_{ij}$ depend parametrically on the nuclear configuration $\mathbf{q}$: $t_{ij}=t_{ij}(\mathbf{q})$, etc.

The CEO algorithm starts with computing the ground-state density matrix which may be obtained by solving the Hartree–Fock equation[62]

$$[F(\overline{\rho}),\overline{\rho}]=0. \tag{A3}$$

The brackets $[\cdots,\cdots]$ denote the commutator of two operators in the Hilbert space. $F=t+\hat{V}\overline{\rho}$ is the Fock operator, which is the sum of the hopping matrix t and the Coulomb matrix $\hat{V}\overline{\rho}$. The linear superoperator $\hat{V}$ is defined by

$$(\hat{V}\xi)_{ij}=\sum_{kl} V_{ij,kl}\xi_{kl}, \tag{A4a}$$

$$V_{ij,kl}=2\langle ik|jl\rangle-\langle ij|kl\rangle, \tag{A4b}$$

where indices i, j, etc. run over a fixed basis set of single-electron atomic orbitals. $\hat{V}$ is Hermitian and preserves the Hermiticity of the matrix on which it acts ($V_{ij,kl}=V_{kl,ij}^*=V_{ji,lk}$):[62]

$$\langle\hat{V}a|b\rangle=\langle a|\hat{V}b\rangle, \tag{A5a}$$

$$(\hat{V}a)^\dagger=\hat{V}a^\dagger. \tag{A5b}$$

Here the scalar product $\langle\cdots\rangle$ of two matrices is defined as $\langle a|b\rangle=\mathrm{tr}(a^\dagger b)$.

For a weak external field, the linearized equation of motion for the time-dependent density matrix reads[67,4]

$$i\,\delta\dot{\rho}=\hat{L}\,\delta\rho+\boldsymbol{\mathcal{E}}(t)[\overline{\rho},\boldsymbol{\mu}], \tag{A6}$$

where the Liouville superoperator $\hat{L}$ is defined by its action on the arbitrary matrix ξ:

$$\hat{L}\xi=[F,\xi]+[\hat{V}\xi,\overline{\rho}]. \tag{A7}$$

Here ξ, F, $\boldsymbol{\mu}$, $\overline{\rho}$ are $N\times N$ matrices, N being the basis set size.

Equation (A6) can be viewed as an equation of motion for a system of coupled externally driven classical harmonic oscillators. The oscillator coordinates are the matrix elements of $\delta\rho$. The eigenmodes ξ_ν of $\hat{L}$ are the ''electronic normal modes'' of the system of coupled electronic oscillators (these should not be confused with the vibrational normal modes) and the eigenfrequencies Ω_ν provide the electronic excitation energies.[4]

In the atomic-orbital representation, diagonal elements $(\xi_\nu)_{ii}$ represent the field-induced charges associated with given atomic orbitals, while the off-diagonal elements give the field-induced coherences, or changes in chemical bonding. The Density–Matrix–Spectral-Moments Algorithm (DSMA)[67] is a numerically efficient scheme for solving the CEO equations and computing the electronic modes and optical spectra.[5]

APPENDIX B: SPECTRAL PROPERTIES OF THE LIOUVILLE OPERATOR

Since the TDHF wave function is represented by a single Slater determinant, the total density matrix $\rho(t)$ must be a projector (idempotent) at all times:

$$[\overline{\rho}+\delta\rho(t)]^2=\overline{\rho}+\delta\rho(t). \tag{B1}$$

Consequently, not all of its matrix elements are independent. The number of degrees of freedom of $\delta\rho$ subject to the condition Eq. (B1) is precisely the number of its particle-hole matrix elements.[67] The projector property of the ground-state density matrix, $\overline{\rho}^2=\overline{\rho}$ splits the total single-particle Hilbert space of dimensionality N into the particle (occupied) and hole (virtual) subspaces of dimensionalities N_p and N_h respectively. The Liouville space of all $N\times N$-dimensional matrices can be then partitioned into the $(N_p^2+N_h^2)$-dimensional subspace of the block-diagonal matrices with respect to the particle and hole subspaces, and the $2N_pN_h$-dimensional subspace of block-off-diagonal matrices. The latter subspace which will be denoted $\mathcal{M}$ is the actual phase-space of the system of electronic oscillators. Any $N\times N$ idempotent density matrix ρ in the vicinity of $\overline{\rho}$ can be uniquely parametrized by its particle-hole block ξ:

$$\rho=\overline{\rho}+\xi+T(\xi). \tag{B2}$$

Here $T(\xi)$ is a block-diagonal matrix containing only the particle–particle and hole–hole matrix elements that can be expressed in terms of ξ as[67]

$$T(\xi)=(1-2\overline{\rho})\frac{1-\sqrt{1-4\xi^2}}{2}$$

$$=(1-2\overline{\rho})\sum_{m=1}^{\infty}\frac{2^m(2m-3)!!}{2m!}\xi^{2m}. \tag{B3}$$

When ξ is small, $T\approx(1-2\overline{\rho})\xi^2$ is quadratic in ξ.

$\mathcal{M}$ is an invariant subspace of $\hat{L}$. Namely, for any block-off-diagonal ξ, $\hat{L}\xi$ is also block-off-diagonal [see Eq. (A7)]. The operator $\hat{L}$ restricted to the $\mathcal{M}$ subspace has $2N_pN_h$ eigenmodes ξ_ν that belong to $\mathcal{M}$. These eigenmodes come in pairs, $\xi_\nu,\xi_\nu^\dagger$ due to the property

$$\hat{L}\xi^\dagger=-(\hat{L}\xi)^\dagger, \tag{B4}$$

which follows directly from the definition Eq. (A7) and Eq. (A5b). The corresponding eigenfrequencies $\pm\Omega_\nu$ differ only in sign.

A scalar product in the space of $N\times N$ matrices can be introduced as $\langle\xi|\eta\rangle=\mathrm{tr}(\xi^\dagger\eta)$. This definition has a drawback since the Liouville operator $\hat{L}$ is not Hermitian with respect to it. Anticipating the need for the perturbative expansion of the eigenmodes of $\hat{L}$, the Hermiticity of the operator $\hat{L}$ is strongly desired. To that end we note that the projector properties of $\overline{\rho}$ allow to introduce a different scalar product on $\mathcal{M}$[88,4]

$$(\xi|\eta)\equiv\mathrm{tr}(\xi^\dagger[\overline{\rho},\eta])=\langle\xi|[\rho,\eta]\rangle. \tag{B5}$$

The Liouville operator is Hermitian with respect to this scalar product:

$$(\hat{L}\xi,\eta)=(\xi,\hat{L}\eta). \tag{B6}$$

Equation (B5) obeys the following properties:

$$(\xi|\eta)=(\eta|\xi)^*=-(\xi^\dagger|\eta^\dagger) \tag{B7}$$

Note that this scalar product is unusual since (ξ,ξ) can be zero for a nonzero matrix ξ. In particular, $(\xi|\xi)=0$ if $\xi=\xi^\dagger$ and $(\xi|\xi^\dagger)=0$ for any ξ. Due to the Hermiticity of $\hat{L}$, its eigenmodes can be chosen orthonormal such that

$$(\xi_\mu|\xi_\nu)=g_\nu\delta_{\mu\nu}, \tag{B8}$$

where $g_\nu=\mathrm{sign}(\Omega_\nu)$. Note that half of the eigenmodes (those with negative eigenfrequencies), also have negative norms.

Using the scalar product Eq. (B5), any block-off-diagonal matrix ξ can be expanded as

$$|\xi)=\sum_\nu g_\nu|\xi_\nu)(\xi_\nu|\xi). \tag{B9}$$

The present bra (ket) notation underlines the similarity with Dirac's Hilbert space.

APPENDIX C: GROUND-STATE ENERGY DERIVATIVES: THE CPHF EQUATIONS

In this Appendix we review the coupled perturbed Hartree–Fock (CPHF) equations which allow to compute derivatives of the HF energy Eq. (11) and the ground-state density matrix Eq. (13).[81–83] In Appendix D we develop an analogous excited-state analytic derivative procedure.

The HF equations for the ground-state density matrix $\overline{\rho}$ and energy E_0 at an arbitrary nuclear configuration are:

$$\overline{\rho}^2=\overline{\rho}, \tag{C1a}$$

$$[F,\overline{\rho}]=0, \tag{C1b}$$

$$E_0=2\,\mathrm{tr}(\overline{\rho}t+\tfrac{1}{2}\overline{\rho}\hat{V}\overline{\rho}). \tag{C1c}$$

Hereafter we denote derivatives with respect to nuclear coordinates by superscripts (e.g., $\overline{\rho}^q\equiv\partial\overline{\rho}/\partial q$). Derivatives of Eqs. (C1a)–(C1c) give the complete system of equations for calculating derivatives of E_0 and $\overline{\rho}$. Taking the derivatives of Eq. (C1a) we obtain

$$\overline{\rho}^q=\overline{\rho}\overline{\rho}^q+\overline{\rho}^q\overline{\rho}. \tag{C2}$$

It immediately follows that $\overline{\rho}^q$ has only particle-hole matrix elements: $\overline{\rho}\overline{\rho}^q\overline{\rho}=(1-\overline{\rho})\overline{\rho}^q(1-\overline{\rho})=0$. Taking derivatives of Eq. (C1c) we obtain Eq. (11). Note that all terms that contain $\overline{\rho}^q$ cancel. Indeed,

$$2\,\mathrm{tr}(\overline{\rho}^q t+\tfrac{1}{2}\overline{\rho}^q\hat{V}\overline{\rho}+\tfrac{1}{2}\overline{\rho}\hat{V}\overline{\rho}^q)=2\,\mathrm{tr}(F\overline{\rho}^q)=0, \tag{C3}$$

since $\overline{\rho}^q$ is block-off-diagonal and F is block-diagonal with respect to the particle and hole subspaces. Thus E_0^q can be readily obtained as soon as the HF equations are solved.

Second derivatives of E_0 can be obtained by an additional differentiation of Eq. (11). However, the terms containing $\overline{\rho}^q$ no longer cancel, and the calculation requires the evaluation of $\overline{\rho}^q$. Differentiating Eq. (C1b), we obtain the following set of linear equations Eq. (13) for $\overline{\rho}^q$. Note that the Liouville operator $\hat{L}$ appears naturally in the left-hand side of Eq. (11). Since $\overline{\rho}^q$ must be Hermitian and should contain only particle-hole matrix elements, only the particle-hole block of the matrix equation Eq. (11) is relevant, which gives a set of $N_p\times N_h$ linear equations for $\overline{\rho}^q$:

$$(\hat{L}\overline{\rho}^q)_{ph}=\widetilde{F^q}_{ph}. \tag{C4}$$

Hereafter $\widetilde{F^q}\equiv(\partial F/\partial q)_{\overline{\rho}}=t^q+\hat{V}^q\overline{\rho}$ denote the partial derivative of the Fock operator at fixed $\overline{\rho}$. In the basis of molecular orbitals, these CPHF equations read:

$$(\epsilon_p-\epsilon_h)\overline{\rho}^q_{ph}-A_{ph,p'h'}\overline{\rho}^q_{p'h'}=\widetilde{F^q}_{ph}, \tag{C5}$$

where $A_{ph,p'h'}=4\langle pp'|hh'\rangle-\langle ph|p'h'\rangle-\langle ph|h'p'\rangle$. Indices p (p') and h (h') run over particle (occupied) and hole (virtual) orbitals, respectively. Using $\overline{\rho}^q$ we can then compute the expectation value of the derivative of any single-electron (such as the dipole) operator:

$$\frac{d}{dq}\langle 0|\boldsymbol{\mu}|0\rangle=\frac{d}{dq}\mathrm{tr}(\overline{\rho}\boldsymbol{\mu})=\mathrm{tr}(\overline{\rho}^q\boldsymbol{\mu})+\mathrm{tr}(\overline{\rho}\boldsymbol{\mu}^q). \tag{C6}$$

APPENDIX D: DERIVATIVES OF THE EXCITED STATE ENERGY: CPCEO EQUATIONS

To develop an analytic derivative procedure for the excited states we start with Eq. (3) and expand the CEO excited-state adiabatic surface and the electronic normal modes in the vicinity of $\mathbf{q}_0$. This results in Eqs. (12) and (14) which we shall denote the Coupled-Perturbed CEO (CPCEO) equations.

We first construct a set of CEO relations[89] analogous to Eqs. (C1) for the ground-state normalization condition for the electronic modes [Eq. (B8)], expression for excitation frequency Ω_ν, and the eigenvalue equation for $\hat{L}\xi_\nu$ [Eq. (3)]

$$(\xi_\nu|\xi_\nu)=1, \tag{D1a}$$

$$\Omega_\nu=(\xi_\nu|\hat{L}|\xi_\nu), \tag{D1b}$$

$$\hat{L}\xi_\nu=\Omega_\nu\xi_\nu. \tag{D1c}$$

We next take the derivative of the normalization condition Eqs. (D1a):

$$(\xi^q_\nu|\xi_\nu)+(\xi_\nu|\xi^q_\nu)+\mathrm{tr}(\overline{\rho}^q[\xi^\dagger_\nu,\xi_\nu])=2(\xi^q_\nu|\xi_\nu)=0. \tag{D2}$$

The third term appears due to the definition of scalar product which depends on $\overline{\rho}$. This term vanishes because $\overline{\rho}^q$ is block-off-diagonal due to Eq. (C2), while $[\xi_\nu^\dagger, \xi_\nu]$ is block-diagonal, and as a result, the trace is zero. Thus, the derivative of the normal mode is orthogonal to the mode itself with respect to the scalar product [Eq. (B5)].

By differentiating the expression for Ω_ν [Eqs. (D1b)], we obtain

$$\Omega_\nu^q = (\xi_\nu | \widetilde{L^q} | \xi_\nu) + (\xi_\nu | \widetilde{L^\rho} | \xi_\nu), \tag{D3}$$

where

$$\widetilde{L^q}\xi = [\widetilde{F^q}, \xi] + [\hat{V}^q \xi, \overline{\rho}], \tag{D4a}$$

$$\widetilde{L^\rho}\xi = [\hat{V}\overline{\rho}^q, \xi] + [\hat{V}\xi, \overline{\rho}^q]. \tag{D4b}$$

The terms with ξ_ν^q cancel due to Eq. (D2) and the Hermiticity property of $\hat{L}$. Eqs. (D3), (D4a), and (D4b) give a closed analytic expression Eq. (12) for Ω_ν^q.

Finally, the derivative of the Eq. (D1c) gives the equation for the derivative of the electronic mode ξ_ν:

$$(\hat{L} - \Omega_\nu)\xi_\nu^q = -(\widetilde{L^q} - \Omega_\nu^q + \widetilde{L^\rho})\xi_\nu. \tag{D5}$$

Substituting Eqs. (D4a) and (D4b) into Eq. (D5) we obtain Eq. (14). This matrix equation represents a system of $2N_pN_h$ equations for the particle-hole elements of the matrix ξ_ν^q. We assume for simplicity that the mode ξ_ν is nondegenerate. In this case the operator $\hat{L} - \Omega_\nu$ has one zero eigenvalue. One of the equations is therefore redundant and should be replaced by the normalization condition, Eq. (D2).

Equation (D5) is formally very similar to the CPHF [Eqs. (C4)] for the derivative of $\overline{\rho}$. The main difference is that the matrix ξ_ν is non-Hermitian, so that both particle-hole and hole-particle components of the matrix equation are needed, which doubles the number of equations. The equation for ξ_ν^q can further be written using the molecular-orbital representation, similar to Eq. (C5):

$$\begin{aligned} (\epsilon_p - \epsilon_h - \Omega_\nu)\xi_{ph}^q - A_{ph,p'h'}\xi_{p'h'}^q &= \zeta_{ph}, \\ (\epsilon_h - \epsilon_p - \Omega_\nu)\xi_{hp}^q - A_{hp,h'p'}\xi_{h'p'}^q &= \zeta_{hp}, \end{aligned} \tag{D6}$$

where ζ is the matrix in the right-hand side of Eq. (D5).

In close analogy with Eq. (C6), ξ_ν^q allows to compute the derivative of the transition matrix element of any single-particle operator and in particular the dipole-moment operator [cf. Eq. (C6)]:

$$\frac{d}{dx}\langle 0 | \boldsymbol{\mu} | \nu \rangle = \frac{d}{dx}\mathrm{tr}(\xi_\nu \boldsymbol{\mu}) = \mathrm{tr}(\xi_\nu^q \boldsymbol{\mu}) + \mathrm{tr}(\xi_\nu \boldsymbol{\mu}^q). \tag{D7}$$

The first derivative of ξ_ν together with the second derivative of $\overline{\rho}$ allows to compute the second derivative of Ω_ν. Taking derivative of Eq. (D3) we obtain

$$\Omega_\nu^{xy} = 2(\xi_\nu^y | \widetilde{L^q} + \widetilde{L^\rho} | \xi_\nu) + (\xi_\nu | \widetilde{L^{xy}} + \widetilde{L^{\rho x}} + \widetilde{L^{\rho y}} + \widetilde{L^{\rho\rho}} | \xi_\nu). \tag{D8}$$

Here the operators $\widetilde{L^{xy}}$, $\widetilde{L^{\rho y}}$, and $\widetilde{L^{\rho\rho}}$ are defined as

$$\widetilde{L^{xy}}\xi = [\widetilde{F^{xy}}, \xi] + [\widetilde{\hat{V}^{xy}}\xi, \overline{\rho}], \tag{D9a}$$

$$\widetilde{L^{\rho y}}\xi = [\hat{V}^y \overline{\rho}^q, \xi] + [\hat{V}^y \xi, \overline{\rho}^q], \tag{D9b}$$

$$\widetilde{L^{\rho\rho}}\xi = [\hat{V}\overline{\rho}^{xy}, \xi] + [\hat{V}\xi, \overline{\rho}^{xy}], \tag{D9c}$$

where the superscripts on $\widetilde{F}$ and $\widetilde{\hat{V}}$, denote partial derivatives at fixed $\overline{\rho}$, which are the input to the calculations.

[1] J. Michl and V. Bonacic-Koutecky, *Electronic Aspects of Organic Photochemistry* (Willey, New York, 1990); M. Klessinger and J. Michl, *Excited States and Photochemistry of Organic Molecules* (VCH, New York, 1995).
[2] E. Deumens, A. Diz, R. Longo, and Y. Ohrn, Rev. Mod. Phys. **66**, 917 (1994).
[3] E. V. Tsiper, V. Chernyak, S. Tretiak, and S. Mukamel, Chem. Phys. Lett. **302**, 77 (1999).
[4] V. Chernyak and S. Mukamel, J. Chem. Phys. **104**, 444 (1996).
[5] S. Mukamel, S. Tretiak, T. Wagersreiter, and V. Chernyak, Science **277**, 781 (1997); S. Tretiak, V. Chernyak, and S. Mukamel, J. Phys. Chem. B **102**, 3310 (1998).
[6] M. Garavelli, P. Celani, F. Bernardi, M. A. Robb, and M. J. Olivucci, J. Am. Chem. Soc. **119**, 6891 (1997); T. Vreven, F. Bernardi, M. Garavelli, M. Olivucci, M. A. Robb, and H. B. Schlegel, J. Am. Chem. Soc. **119**, 12687 (1997).
[7] G. Wald, Science **162**, 230 (1968).
[8] G. G. Kochendoerfer and R. A. Mathies, Isr. J. Chem. **35**, 211 (1995).
[9] K. Schulten, W. Humphrey, I. Logunov, M. Sheves, and D. Xu, Isr. J. Chem. **35**, 447 (1995).
[10] R. R. Birge, Biochim. Biophys. Acta **1016**, 293 (1989).
[11] S. Mukamel, *Principles of Nonlinear Optical Spectroscopy* (Oxford University Press, Oxford, 1995).
[12] V. F. Kamalov, T. M. Masciangioli, and M. A. El-Sayed, J. Phys. Chem. **100**, 2762 (1996).
[13] H. Houjou, Y. Inoue, and M. Sakurai, J. Am. Chem. Soc. **120**, 4459 (1998).
[14] S. W. Lin, M. Groesbeek, I. van der Hoef, P. Verdegem, J. Lugtenburg, and R. A. Mathies, J. Phys. Chem. B **102**, 2787 (1998).
[15] H. Kandori, N. Kinoshita, Y. Shichida, and A. Maeda, J. Phys. Chem. B **102**, 7899 (1998).
[16] E. Schmalzlin, K. Meerholz, S. Stadler, C. Brauchle, H. Patzelt, and D. Oesterhelt, Chem. Phys. Lett. **280**, 551 (1997).
[17] R. R. Birge, C. F. Zhang, J. Chem. Phys. **92**, 7178 (1990).
[18] S. L. Logunov, T. M. Masciangioli, V. F. Kamalov, and M. A. El-Sayed, **102**, 2303 (1998).
[19] F. Gai, K. C. Hasson, J. C. McDonald, and P. A. Anfinrud, Science **279**, 1886 (1998).
[20] F. Gai, J. C. McDonald, and P. A. Anfinrud, J. Am. Chem. Soc. **119**, 6201 (1997).
[21] K. C. Hasson, F. Gai, and P. A. Anfinrud, Proc. Natl. Acad. Sci. USA **93**, 15124 (1996).
[22] Q. Wang, G. G. Kochendoerfer, R. W. Schoenlein, P. J. E. Verdegem, J. Lugtenburg, R. A. Mathies, and C. V. Shank, J. Phys. Chem. **100**, 17388 (1996).
[23] Q. Wang, R. W. Schoenlein, L. A. Peteanu, R. A. Mathies, and C. S. Shank, Science **266**, 422 (1994).
[24] R. W. Schoenlein, L. A. Peteanu, Q. Wang, R. A. Mathies, and C. V Shank, J. Phys. Chem. **97**, 12087 (1993).
[25] L. A. Peteanu, R. W. Schoenlein, Q. Wang, R. A. Mathies, and C. W. Schank, Proc. Natl. Acad. Sci. USA **90**, 11762 (1993).
[26] R. W. Schoenlein, L. A. Peteanu, R. A. Mathies, and C. V. Shank, Science **254**, 412 (1991).
[27] M. Yan, D. Manor, G. Weng, H. Chao, L. Rothberg, T. M. Jedju, R. R. Alfano, and R. H. Callender, Proc. Natl. Acad. Sci. USA **88**, 9809 (1991).
[28] T. Kobayashi, M. Kim, M. Taiji, T. Iwasa, M. Nakagawa, and M. Tsuda, J. Phys. Chem. **102**, 272 (1998).
[29] S. Yamaguchi and H. Hamaguchi, J. Chem. Phys. **109**, 1397 (1998); S. Yamaguchi and H. Hamaguchi, Chem. Phys. Lett. **287**, 695 (1998).
[30] C. J. Bardeen, Q. Wang, and C. V. Shank, J. Phys. Chem. A **102**, 2759 (1998).
[31] R. Diller, Chem. Phys. Lett. **295**, 47 (1998).
[32] G. G. Kochendoerfer and R. A. Mathies, J. Phys. Chem. **100**, 14526 (1996).
[33] D. Wexler, G. G. Kochendoerfer, and R. A. Mathies, in *Femtochemistry*

and Photobiology Nobel Symposium 101, edited by V. Sungstrom (Imperial College Press, London, 1997), p. 724.
[34] H. Chosrowjan, N. Mataga, Y. Shibata, S. Tachibanaki, H. Kandori, Y. Shichida, T. Okada, and T. Kouyama, J. Am. Chem. Soc. **120**, 9706 (1998).
[35] S. Takeuchi and T. Tahara, J. Phys. Chem. **101**, 3052 (1997).
[36] L. Song and M. A. El-Sayed, J. Am. Chem. Soc. **120**, 8889 (1998).
[37] F. Jager, L. Ujj, and G. H. Atkinson, J. Am. Chem. Soc. **119**, 12610 (1997).
[38] B. H. Green, T. G. Monger, and R. R. Alfano, B. Aton, and R. H. Callender, Nature (London) **269**, 179 (1977); A. G. Doukas, V. Stefancic, T. Suzuki, R. H. Callender, and R. R. Alfano, Photobiochem. Photobiophys. **1**, 305 (1980).
[39] I. Rousso, Y. Gat, A. Lewis, M. Sheves, and M. Ottolenghi, Biophys. J. **75**, 413 (1998).
[40] W. Hage, M. Kim, H. Frei, and R. A. Mathies, J. Phys. Chem. **100**, 16026 (1996).
[41] D. Xu, C. Martin, and K. Schulten, Biophys. J. **70**, 453 (1996).
[42] W. Humphrey, D. Xu, M. Sheves, and K. Schulten, J. Phys. Chem. **99**, 14549 (1995).
[43] G. Haran, K. Wynne, A. Xie, Q. He, M. Chance, and R. M. Hochstrasser, Chem. Phys. Lett. **261**, 389 (1996).
[44] W. Humphrey, H. Lu, I. Logunov, H.-J. Werner, and K. Schulten, Biophys. J. **75**, 1689 (1998).
[45] W. Domcke and G. Stock, Adv. Chem. Phys. **100**, 1 (1997).
[46] M. A. Robb, F. Bernardi, M. Olivucci, Pure Appl. Chem. **67**, 783 (1995).
[47] M. Garavelli, T. Vreven, P. Celani, F. Bernardi, M. A. Robb, and M. Olivucci, J. Am. Chem. Soc. **120**, 1285 (1998), and earlier references therein.
[48] M. Garavelli, P. Celani, F. Bernardi, M. A. Robb, and M. Olivucci, J. Am. Chem. Soc. **119**, 11 487 (1997); F. Bernardi, M. Olivucci, and M. A. Robb, Chem. Soc. Rev. **321**, (1996); M. Garavelli, P. Celani, N. Yamamoto, F. Bernardi, M. A. Robb, and M. Olivucci, J. Am. Chem. Soc. **118**, 11656 (1996).
[49] M. Del. Zoppo, C. Castiglioni, P. Zuliani, and G. Zerbi, in *Handbook of Conducting Polymers*, edited by T. A. Skotheim, R. L. Elsenbaumer, and J. Reynolds (Dekker, New York, 1998).
[50] A. Bifone, H. J. M. deGroot, and F. Buda, Pure Appl. Chem. **69**, 2105 (1997); G. La Penna, F. Buda, A. Bifone, and H. J. M. de Groot, Chem. Phys. Lett. **294**, 447 (1998).
[51] W. Humphrey, E. Bamberg, and K. Schulten, Biophys. J. **72**, 1347 (1997).
[52] I. Logunov, W. Humphrey, K. Schulten, and M. Sheves, Biophys. J. **68**, 1270 (1995).
[53] R. Car and M. Parinello, Phys. Rev. Lett. **55**, 2471 (1985); For a review see, e.g., D. K. Remler and P. A. Madden, Mol. Phys. **70**, 921 (1990).
[54] R. McWeeny and B. T. Sutcliffe, *Methods of Molecular Quantum Mechanics* (Academic, New York, 1976); E. R. Davidson, *Reduced Density Matrices in Quantum Chemistry* (Academic, New York, 1976).
[55] P. Hohenberg and W. Kohn, Phys. Rev. **136**, B864 (1964).
[56] W. Kohn and L. J. Sham, Phys. Rev. **140**, A1133 (1965).
[57] J. A. Pople, P. M. W. Gill, and B. J. Johnson, Chem. Phys. Lett. **199**, 557 (1992).
[58] A. D. Becke, Phys. Rev. A **38**, 3098 (1988).
[59] E. K. U. Gross, J. F. Dobson and M. Petersilka, in *Density Functional Theory*, edited by R. F. Nalewajski (Springer, Berlin, 1996), Vol. 181, pp. 1–81.
[60] M. E. Casida, in *Recent Advances in Density-Functional Methods*, Part I, edited by D. A. Chong (World Scientific, Singapore, 1995), Vol. 3, pp. 155–192.
[61] C. Jamorski, M. E. Casida, and D. R. Salahub, J. Chem. Phys. **104**, 5134 (1996).
[62] A. Szabo and N. S. Ostlund, *Modern Quantum Chemistry: Introduction to Advanced Electronic Structure Theory* (McGraw-Hill, New York, 1989).
[63] P. Ring and P. Schuck, *The Nuclear Many-Body Problem* (Springer-Verlag, New York, 1980).
[64] S. Tretiak, V. Chernyak, and S. Mukamel, Int. J. Quantum Chem. **70**, 711 (1998).
[65] M. J. Frisch *et al.*, GAUSSIAN 94 (Gaussian Inc, Pittsburgh, 1995).
[66] J. Ridley and M. C. Zerner, Theor. Chim. Acta **32**, 111 (1973); M. C. Zerner, G. H. Loew, R. F. Kirchner, and U. T. Mueller-Westerhoff, J. Am. Chem. Soc. **102**, 589 (1980).
[67] S. Tretiak, V. Chernyak, and S. Mukamel, J. Am. Chem. Soc. **119**, 11408 (1997).
[68] Due to the lack of full σ_s symmetry, all transitions are formally allowed, however the oscillator strengths for the A_g-like transitions are about 10 times smaller.
[69] Z. G. Soos, S. Ramasesha, and D. S. Galvao, Phys. Rev. Lett. **71**, 1609 (1993); Z. G. Soos, Mol. Cryst. Liq. Cryst. **256**, 35 (1994).
[70] B. E. Kohler and T. A. Spiglanin, J. Chem. Phys. **80**, 23 (1984); W. J. Buma, B. E. Kohler, and K. Song, J. Chem. Phys. **94**, 6367 (1991).
[71] A single DSMA calculation takes 4 s for the present small molecule, while a similar calculation on CIS 6-31+G level using Gaussian 94 takes 40 s. The timing results are for a single R10000 processor of SGI Octane workstation. The comparison becomes more favorable for larger molecules.
[72] G. E. Forsythe, M. A. Malcolm, and C. B. Moler, *Computer Methods for Mathematical Computations* (Prentice-Hall, Englewood Cliffs, N.J., 1977).
[73] The timing results are for a single R10000 processor of SGI Octane workstation.
[74] G. C. Bazan, W. J. Oldham, R. J. Lachicotte, S. Tretiak, V. Chernyak, and S. Mukamel, J. Am. Chem. Soc. **120**, 9188 (1998).
[75] J. Baker and M. Zerner, Chem. Phys. Lett. **175**, 192 (1990).
[76] S. Tretiak, V. Chernyak, and S. Mukamel, Chem. Phys. Lett. **287**, 75 (1998).
[77] M. Ben-Nun and T. J. Martinez, Chem. Phys. Lett. **298**, 57 (1998); *ibid.* **290**, 189 (1998).
[78] E. Neriya, S. Fischer, and M. Karplus, J. Chem. Phys. **105**, 1902 (1996).
[79] B. R. Brooks, R. E. Bruccoleri, B. D. Olafson, D. J. States, S. Swamintha, and M. Karplus, J. Comput. Chem. **4**, 187 (1983).
[80] M. W. Schmidt *et al.*, GAMESS, J. Comput. Chem. **14**, 1347 (1993).
[81] R. M. Stevens, R. M. Pitzer, and W. N. Lipscomb, J. Chem. Phys. **38**, 550 (1963).
[82] J. A. Pople, R. Krishnan, H. B. Schlegel, and J. S. Binkley, Int. J. Quantum Chem., Quantum Chem. Symp. **13**, 225 (1979).
[83] M. J. Frisch, Y. Yamaguchi, J. F. Gaw, and H. F. Schaefer III, J. Chem. Phys. **84**, 531 (1985); Y. Yamaguchi, M. Frisch, J. Gaw, and H. F. Schaefer III, *ibid.*, **84**, 2262 (1986). M. J. Frisch, M. Head-Gordon, and J. A. Pople, Chem. Phys. Lett. **141**, 189 (1990); *ibid.* **166**, 275 (1990); *ibid.* **166**, 281 (1990).
[84] S. Tretiak, V. Chernyak, and S. Mukamel, J. Chem. Phys. **105**, 8914 (1996).
[85] O. Dubovsky, S. Mukamel, J. Chem. Phys. **95**, 7828 (1991).
[86] E. Schwegler, M. Challacombe, M. Head-Gordon, J. Chem. Phys. **106**, 9708 (1997); M. C. Strain, G. E. Scuseria, M. J. Frisch, Science **271**, 5245 (1996).
[87] X. P. Li, W. Nunes, and D. Vanderbilt Phys. Rev. B **47**, 10891 (1993).
[88] D. J. Thouless, Nucl. Phys. **22**, 78 (1961).
[89] All equations in this Appendix are based on the spectral properties of Liouville superoperator, outlined in the Appendix B. In particular, the scalar product used here is defined by Eq. (B5).